Mwangi et al. *Zool. Res.* 2025, 46(5): 1203−1218
https://doi.org/10.24272/j.issn.2095-8137.2025.303
https://cstr.cn/32248.14.zr.2025.303

ZR | Zoological Research

Article Open Access

Integrating a cationic backbone with a hydrophobic core: A structure-function strategy for designing self-assembling antimicrobial peptides with enhanced activity

James Mwangi[1,2,#], Dawit Adisu Tadese[1,2,#], Yi Wang[1,3], Demeke Asmamaw[1,2], Min Yang[1,2], Brenda. B. Michira[1,2], Mehwish Khalid[1,2], Zi-Yi Wang[1,2], Qiu-Min Lu[1,2], Ren Lai[1,2,3,*]

[1] *Engineering Laboratory of Peptides of Chinese Academy of Sciences*, *Key Laboratory of Bioactive Peptides of Yunnan Province*, *KIZ-CUHK Joint Laboratory of Bioresources and Molecular Research in Common Diseases*, *National Resource Center for Non-Human Primates*, *National Research Facility for Phenotypic & Genetic Analysis of Model Animals (Primate Facility)*, *State Key Laboratory of Genetic Evolution & Animal Models*, *Sino-African Joint Research Center*, *and New Cornerstone Science Laboratory*, *Kunming Institute of Zoology*, *Chinese Academy of Sciences*, *Kunming*, *Yunnan* 650201, *China*

[2] *Kunming College of Life Science*, *University of Chinese Academy of Sciences*, *Kunming* 650204, *China*

[3] *Center for Evolution and Conservation Biology*, *Southern Marine Science and Engineering Guangdong Laboratory (Guangzhou)*, *Guangzhou*, *Guangdong* 511458, *China*

ABSTRACT

Effective countermeasures against multidrug-resistant nosocomial pathogens, such as carbapenem-resistant *Klebsiella pneumoniae* and methicillin-resistant *Staphylococcus aureus* (MRSA), require the development of innovative antimicrobial strategies. This study presents a structure-function approach to antimicrobial peptide (AMP) design through the strategic integration of a cationic backbone with a hydrophobic core. This dual-domain architecture enables robust hydrophobic and electrostatic interactions, promoting spontaneous self-assembly and efficient membrane engagement. The lead peptide, Tryptolycin (TRPY), formed stable, monodisperse nanoparticles and demonstrated broad-spectrum bactericidal activity, with minimum inhibitory concentrations ≤1 μmol/L against multiple strains of MRSA and *K. pneumoniae*, while exerting minimal cytotoxicity toward mammalian cells. TRPY achieved rapid bacterial elimination, eradicating 99.9% of both planktonic and persister populations within minutes. Mechanistic investigations revealed that TRPY induced membrane permeabilization, promoted reactive oxygen species (ROS) production, and inhibited biofilm formation. In murine infection models, TRPY effectively eradicated established infections, reducing bacterial burden across target organs by 3- to 5-fold without significant cytotoxicity at therapeutic concentrations. Collectively, these findings establish TRPY as a promising therapeutic agent for clinical translation in the treatment of refractory bacterial infections.

Keywords: Self-assembly; Antimicrobial peptides; Nosocomial pathogens; Antibiotic resistance

INTRODUCTION

Infections caused by multidrug-resistant pathogens such as carbapenem-resistant *Klebsiella pneumoniae* and methicillin-resistant *Staphylococcus aureus*, now classified as “critical priority pathogens” by the World Health Organization, present a growing clinical challenge marked by increased mortality, prolonged hospitalization, and escalating healthcare costs (Duan et al., 2025). Despite decades of research, few antibiotics have reached clinical use, and resistance continues to erode the efficacy of existing agents (Kim et al., 2022; Meinberger et al., 2023). Addressing this urgent situation requires a radical shift toward therapeutics that not only exhibit

Received: 04 August 2025; Accepted: 27 August 2025; Online: 28 August 2025

Foundation items: This work was supported by the National Key Research and Development Program of China (2022YFC2105003, 2022YFC2602500), National Natural Science Foundation of China (92469103, 32400769, 32300404), Chinese Academy of Sciences (YSBR-111, SAJC202402), Yunnan Provincial Science and Technology Department (202305AH340007, 202301AT070343, 202502AA310005), Yunnan Characteristic Plant Extraction Laboratory (2025YKZY002), Kunming Science and Technology Bureau (2022SCP007), New Cornerstone Investigator Program from Shenzhen New Cornerstone Science Foundation (NCI202238), Tianfu Jincheng Laboratory Foundation (TFJC2023010007), and Chinese Academy of Sciences and World Academy of Sciences (CAS-TWAS) President’s Fellowship Program (2019A8010415001)

[#]Authors contributed equally to this work

*Corresponding author, E-mail: rlai@mail.kiz.ac.cn

potent, broad-spectrum antimicrobial activity but also circumvent conventional resistance mechanisms (Wu et al., 2024).

As evolutionarily conserved immune effectors, antimicrobial peptides (AMPs) have long been recognized for their membrane-targeting activity and reduced likelihood of resistance development, thereby representing attractive scaffolds for next-generation antibiotics (Huang & Li, 2023; Mwangi et al., 2023). However, clinical translation has been hindered by susceptibility to proteolytic degradation, off-target cytotoxicity, and limited efficacy under physiological conditions (Mwangi et al., 2023). Recent advances in peptide engineering have focused on rational design strategies to enhance their selectivity, self-assembly, and multifunctionality (Okesola & Mata, 2018; Sinha et al., 2021). Incorporation of aromatic residues, such as tryptophan, has proven especially effective due to their membrane-interacting capabilities, facilitating nanostructure formation and antimicrobial potency (Balasco et al., 2024; Zhang et al., 2020). Peptide-based materials have also shown therapeutic versatility across biomedical disciplines. In cancer therapy, AMPs have been adapted as nanocarriers for targeted drug delivery, activated within tumor microenvironments, and used to induce apoptosis in malignant cells via membrane lysis (Deslouches & Di, 2017; Zare-Zardini et al., 2024). In regenerative medicine, bioactive peptides have shown promise in tissue engineering applications, promoting cell adhesion, proliferation, and differentiation while providing structural support for tissue regeneration (Li et al., 2025). Self-assembling peptides have additionally enhanced vaccine platforms, serving as adjuvants and delivery vehicles for antigen exposure and immune potentiation (Hamley, 2022; Skwarczynski & Toth, 2016). These applications collectively underscore the translational potential of rationally engineered peptide assemblies, providing valuable insights that can inform the development of next-generation antimicrobial peptides.

Self-assembly of membrane-targeting peptides is a conserved antimicrobial strategy observed across all domains of life (Eisenberg & Sawaya, 2017). Many organisms, including humans, secrete membrane-targeting AMPs as a critical component of the immune response (Bulet et al., 2004). For example, human cathelicidin peptide LL-37 (Sancho-Vaello et al., 2020), human α-defensin 6 (Chu et al., 2012), and protegrin-1 (Chairatana & Nolan, 2017) can self-assemble into supramolecular or fibrillar structures, thereby enhancing their antimicrobial and immunological activity (Eisenberg & Sawaya, 2017). Several AMPs initiate antimicrobial action via specific binding and oligomerization on microbial surface components such as lipopolysaccharide (LPS) and lipoteichoic acid (LTA), a process thought to facilitate membrane targeting and peptide activation (Sancho-Vaello et al., 2017; Shahmiri et al., 2016). These peptide assemblies resemble classical amyloids—highly stable, unbranched fibrillar structures characterized by cross-β-sheet arrangements stabilized through hydrogen bonding, hydrophobic forces, and π-π interactions (Greenwald & Riek, 2010; Rambaran & Serpell, 2008; Wang et al., 2016). Notably, both amphipathic AMPs and amyloid-related short peptides frequently contain a large number of aromatic amino acids, which appear to accelerate the formation of stable functional assemblies (Glossop et al., 2019). Integration of AMP-mediated antimicrobial activity with the structural advantages of self-assembled nanostructures offers a promising strategy to overcome the limitations that hinder their clinical application.

This study introduces Tryptolycin (TRPY), a *de novo* engineered, amphipathic peptide enriched in tryptophan residues and designed to self-assemble into stable nanoparticles with potent antimicrobial activity. The design features strategically arrayed cationic and aromatic residues that promote selective interaction with bacterial membranes, facilitate self-assembly through π-π stacking interactions, and enhance functional versatility. TRPY exerts multimodal antibacterial effects and combats drug-resistant pathogens via membrane disruption, reactive oxygen species generation, DNA binding, lipopolysaccharide neutralization, and biofilm inhibition. The remarkable efficacy of TRPY against clinically relevant multidrug-resistant (MDR) pathogens, together with its favorable safety profile, supports its considerable potential as a therapeutic candidate for addressing the escalating crisis of antimicrobial resistance (AMR).

MATERIALS AND METHODS

Ethics statement

All experimental procedures were conducted in accordance with protocols approved by the Institutional Review Board of the Kunming Institute of Zoology. Animal experiments received approval from and followed the guidelines of the Animal Care and Use Committee of the Kunming Institute of Zoology, Chinese Academy of Sciences (Approval no. IACUC-RE-2024-12-007).

Peptide synthesis and characterization

Peptides were synthesized by Synpeptide Co., Ltd. (China) using solid-phase peptide synthesis based on Fmoc chemistry. Peptide purity was confirmed to exceed 95% by reversed-phase high-performance liquid chromatography (RP-HPLC). Molecular weights were validated by matrix-assisted laser desorption/ionization time-of-flight mass spectrometry (MALDI-TOF MS).

Transmission electron microscopy (TEM) of self-assembled structure

To examine nanostructure morphology, TRPY was dissolved in phosphate-buffered saline (100 μmol/L, pH 7.4) and applied to carbon-coated copper grids. After 5 min adsorption, excess solution was removed by blotting with filter paper, followed by negative staining with 2% (w/v) uranyl acetate for 2 min. Grids were air-dried and imaged using a JEOL JEM-2100F transmission electron microscope at an accelerating voltage of 200 kV. Images were acquired at magnifications of 6 800× and 21 000× to assess nanostructure dimensions and morphological features. Identical procedures were repeated after co-incubation of the peptide with 10% LPS or LTA to assess the influence of cell wall components on peptide self-assembly.

Determination of antimicrobial activity

Bacterial strains were cultured in Mueller-Hinton broth (MHB) at 37°C for 18–24 h prior to antimicrobial susceptibility testing. The antimicrobial activity of TRPY was determined by broth microdilution assays in RPMI 1640 medium, following Clinical and Laboratory Standards Institute (CLSI) guidelines.

Proteolytic stability assay

To assess proteolytic resistance, TRPY (1 mg/mL) was incubated with chymotrypsin or trypsin (enzyme:peptide ratio

1:50 w/w) in 100 mmol/L Tris-HCl buffer (pH 7.4) at 37°C. Aliquots were collected at 0, 30, 60, 120, 240, and 360 min, and reactions were quenched with 5% trifluoroacetic acid (TFA). Samples were analyzed by HPLC.

Plasma stability assay

To evaluate functional stability in plasma, TRPY (1 mg/mL) was incubated with 0, 12.5, 25, and 50% mouse plasma at 37°C. Aliquots were collected at 0, 1, 2, 4, and 6 h, diluted in RPMI 1640 medium with 10% fetal bovine serum (FBS) to achieve final peptide concentrations ranging from 0.125 to 100 μmol/L. Minimum inhibitory concentration (MIC) assays were performed against *K. pneumoniae* (strain 9409) and MRSA (strain 33564) as described previously (Mwangi et al., 2019).. Control experiments were conducted using TRPY incubated under the same conditions but without enzymes. MIC values were determined after 18–24 h of incubation at 37°C.

Salt sensitivity assay

To examine the effect of physiological salts on antimicrobial activity, MIC values were determined in RPMI-1640 medium supplemented with 150 mM $FeCl_3$, $CaCl_2$, KCl, NaCl, or $MgCl_2$. Assays were conducted against *K. pneumoniae* (strain 9409) and MRSA (strain 33564), with MICs determined after 18–24 h of incubation at 37°C. Control experiments were conducted in unsupplemented RPMI 1640 medium.

Hemolytic activity assay

Hemolytic activity was evaluated using freshly isolated mouse red blood cells (mRBCs) following a previously described protocol (Mwangi et al., 2019).

Cytotoxicity assessment

TRPY-induced cytotoxicity was assessed using three mammalian cell lines: HaCaT (human keratinocytes), RAW264.7 (murine macrophages), and HEK293 (human embryonic kidney cells). Cells were cultured in Dulbecco's Modified Eagle's Medium (DMEM) supplemented with 10% FBS, 100 U/mL penicillin, and 100 μg/mL streptomycin at 37°C in a humidified atmosphere containing 5% CO_2. Following seeding at 1×10^4 cells per well in 96-well plates, cells were allowed to adhere for 24 h. Subsequently, the culture medium was exchanged with serum-free DMEM containing TRPY, LL-37, or magainin 2 at concentrations ranging from 2.5 to 80 μmol/L. After 24 h of treatment, cell viability was assessed using the Cell Counting Kit-8 (CCK-8) assay.

Time-kill kinetics

The bactericidal kinetics of TRPY were assessed against MRSA (strain 33564) and *K. pneumoniae* (strain 9409). Bacteria were adjusted to 1×10^7 colony-forming units (CFU)/mL in RPMI 1640 supplemented with 10% FBS. TRPY was added at 2× MIC concentrations (2 μmol/L), and gentamicin (20 μmol/L) was used as a reference control. Untreated cultures served as negative controls. Cultures were incubated at 37°C with orbital shaking at 200 rpm. Samples (100 μL) were collected at designated intervals (0, 30, 60, 90, 120, 150, 180, 210, 240, 270, 300, 330, and 360 min), serially diluted in sterile saline, and plated onto Mueller-Hinton agar. Viable colony counts were determined following 24-h incubation at 37°C. Killing kinetics were plotted as $\log_{10}$ CFU/mL versus time.

Fluorescence microscopy

TRPY-induced membrane permeabilization was visualized using fluorescence microscopy. MRSA (strain 33564) and *K. pneumoniae* (strain 9409) cultures were cultivated to exponential phase (optical density at 600 nm (OD_{600})=0.5) in Mueller-Hinton broth, collected via centrifugation at 3500 r/min for 5 min at 4 °C, and washed twice in PBS (pH 7.4). Bacterial pellets were reconstituted in PBS to OD_{600}=0.5 and treated with TRPY at 2× MIC for 30 min at 37°C. PBS-treated bacteria served as negative controls. Following treatment, cells were stained with SYTOX Green (2 μmol/L) and propidium iodide (PI, 10 μg/mL) for 15 min at room temperature in the dark. After washing with PBS, stained cells were mounted on glass slides and imaged using a Leica TCS SP8 confocal laser scanning microscope. Fluorescence settings were: SYTOX Green (excitation: 488 nm, emission: 500–550 nm) and PI (excitation: 535 nm, emission: 615–640 nm). Image analysis was conducted using ImageJ.

Flow cytometry

Membrane permeabilization was further quantified using flow cytometry. Both *K. pneumoniae* (strain 9409) and MRSA (strain 33564) were prepared as described above. Stained cells were analyzed on a BD FACSCalibur flow cytometer with 488 nm excitation. Fluorescence signals were collected using FL1 (530 nm) for SYTOX Green and FL2 (585 nm) for PI. Data acquisition included 10 000 events per sample, with subsequent analysis performed using FlowJo.

Membrane depolarization assessment

Membrane depolarization induced by TRPY was evaluated using the potential-sensitive fluorescent probe $DiSC_3(5)$. Both *K. pneumoniae* (strain 9409) and MRSA (strain 33564) were grown to the exponential phase (OD_{600}=0.5) in Mueller-Hinton broth, harvested by centrifugation at 3500 r/min for 5 min at 4°C, and washed twice in 5 mM HEPES buffer (pH 7.4) supplemented with 20 mM glucose. Bacterial suspensions were adjusted to an OD_{600} of 0.05 in the same buffer. $DiSC_3(5)$ was introduced at a final concentration of 2 μmol/L, followed by incubation for 30 min at room temperature to facilitate dye incorporation and fluorescence self-quenching. Membrane potential was equilibrated by the addition of KCl (100 mmol/L final concentration). Cell suspensions were transferred to black 96-well microplates for baseline fluorescence measurement using a microplate reader (excitation, 622 nm; emission, 670 nm). TRPY was introduced at concentrations of 1, 2, 4, and 8 μmol/L, with continuous fluorescence monitoring over a 30 min period.

Scanning electron microscopy (SEM) and TEM

Morphological changes induced by TRPY were visualized using SEM and TEM, following established procedures (Mwangi et al., 2019).

LPS and LTA displacement assay

TRPY binding to LPS and LTA was evaluated using a BODIPY-based fluorescence displacement assay. LPS or LTA (50 μg/mL) was incubated with BODIPY-TR-cadaverine (5 μmol/L) for 6 h at room temperature to form a stable complex. Test compounds (TRPY, LL37, PMB, or vancomycin) were then added at concentrations ranging from 0 to 64 μmol/L in 50 mmol/L Tris buffer (pH 7.4) and incubated for 30 min at 37°C. Fluorescence intensity was quantified using a microplate reader with an excitation wavelength of 580 nm and emission wavelength of 620 nm.

TEM of TRPY-LPS interactions

Direct visualization of LPS-TRPY binding was accomplished

through TEM. In brief, LPS preparations (500 μg/mL) were combined with TRPY (10 μg/mL) and incubated for 1 h at 37°C. Parallel control samples contained LPS alone. Samples were deposited onto carbon-coated copper grids, contrast-enhanced with 1% uranyl acetate negative staining, and observed using TEM at 80 kV accelerating voltage.

Inhibition of LPS-induced inflammatory response in RAW264.7 macrophages

RAW264.7 macrophages were seeded at 1×10^6 cells per well in 24-well culture plates and allowed to adhere overnight. Cells were pre-treated with TRPY (8 μmol/L), LL-37 (8 μmol/L), or colistin (8 μmol/L) for 1 h before LPS stimulation (100 ng/mL) for 12 h. Untreated controls were processed in parallel. Following incubation, culture medium was harvested and centrifuged at 3 000 r/min for 10 min, 4 °C to eliminate cellular debris. Pro-inflammatory cytokine concentrations (IL-1β, TNF-α, and IL-6) in the resulting supernatants were quantified using commercial enzyme-linked immunosorbent assay (ELISA) kits according to the manufacturer's protocols.

Biofilm formation and eradication

The ability of TRPY to inhibit and eradicate biofilms formed by MRSA and *K. pneumoniae* was evaluated using crystal violet staining, as described previously (Mwangi et al., 2019).

Anti-persister activity

TRPY activity against bacterial persisters was assessed by colony enumeration. Persister cells were generated by treating exponential-phase cultures with a high concentration of conventional antibiotics (colistin for *K. pneumoniae* and vancomycin for MRSA at 50× MIC) for 6 h. Surviving cells were collected by centrifugation (10 min at 4 000 r/min, 4°C), washed twice with PBS, and resuspended in fresh Mueller-Hinton broth to approximately 1×10^7 CFU/mL. The persister cells were then exposed to increasing concentrations of TRPY at multiples of MIC for 1 h at 37°C, followed by serial dilutions and plating on Mueller-Hinton agar for CFU quantification.

Efficacy of TRPY in acute *K. pneumoniae* pulmonary infection

Female CD-1 mice (8–10 weeks old, 25–30 g) were intranasally inoculated with the clinical strain *K. pneumoniae* R62 under light isoflurane anesthesia to establish an acute pulmonary infection model. At 2 h post-infection, mice (n=7 per group) received intranasal administration of 2 mg/kg TRPY, 2 mg/kg colistin (positive control), or PBS (vehicle control). At 18 h post-treatment, mice were euthanized through CO_2 asphyxiation, and lungs were harvested for bacterial load quantification via CFU enumeration after homogenization and serial dilution. Blood was collected for serum cytokine analysis (MCP-1, IL-6, TNF-α, and IL-1β) using commercial ELISA kits. Lung tissues were fixed in formalin for histopathological evaluation.

Efficacy of TRPY in an MRSA peritoneal infection

To evaluate the efficacy of TRPY against Gram-positive pathogens, female CD-1 mice (8–10 weeks old) were intraperitoneally injected with MRSA (1×10^8 CFU/mL). At 2 h post-infection, mice (n=6 per group) received 10 mg/kg TRPY or PBS (vehicle control) via intraperitoneal injection. At 24 h post-infection, peritoneal lavage fluid, liver, and kidneys were collected. Bacterial loads in these tissues were quantified via CFU counts after homogenization and plating on selective agar. Liver and kidney samples were fixed in formalin for histopathological evaluation.

Efficacy of TRPY in LPS-induced endotoxemia

Systemic anti-inflammatory activity of TRPY was evaluated in an LPS-induced endotoxemia model. Female CD-1 mice (8–10 weeks old) were intravenously injected with 10 mg/kg *E. coli* LPS to trigger systemic inflammation. At 1 h post-challenge, mice (n=5) received 10 mg/kg TRPY, LL-37, or colistin via intraperitoneal injection. Blood was collected 6 h after LPS administration, and serum cytokine levels (IL-6, MCP-1, TNF-α, and IL-1β) were quantified using ELISA kits according to the manufacturer's instructions (Dakewe Biotech, China).

Data analysis

Unless stated otherwise, all data are expressed as mean±standard error of the mean (SEM). Sample sizes (n) for each experimental condition and statistical analysis are provided in the corresponding figure legends and results section. Statistical comparisons were performed using one-way analysis of variance (ANOVA) with Dunnett's *post hoc* test for multiple comparisons against the control group. All statistical analyses were carried out using GraphPad Prism v.10.0 (GraphPad Software, USA), with P<0.05 considered significant.

RESULTS

Design and self-assembly properties of Tryptolycin

A *de novo* design approach was employed to engineer a class of membrane-disruptive, self-assembling peptides (AP1–AP6) by integrating two synergistic structural features: a cationic amphipathic peptide backbone and a tryptophan (W)-rich hydrophobic core (Figure 1A; Supplementary Table S1). Each peptide was composed of 15–22 amino acids, a range selected to balance bioactivity and synthetic complexity. A net positive charge of +7 to +11 was introduced through strategically spaced lysine (K) and arginine (R) residues, arranged to cluster on one face of the helical structure, thereby enabling electrostatic interactions with negatively charged bacterial membranes. On the opposing face, multiple tryptophan residues formed a densely packed tryptophan (W)-rich hydrophobic domain designed to promote π–π stacking interactions and facilitate spontaneous self-assembly into nanostructures. The resulting amphipathic architecture produced a high hydrophobic moment (<μH>) to enhance membrane targeting, while the average hydrophobicity (H) value was fine-tuned between 0.200 and 0.420 to balance membrane insertion with host cell compatibility. Additionally, to further enhance biocompatibility, a short polyethylene glycol (PEG_2) moiety was appended to the C-terminus to reduce hemolytic activity without compromising antimicrobial efficacy. Initial screening of hemolytic and antimicrobial properties (Supplementary Figure S1 and Table S2) identified AP2—subsequently named Tryptolycin (TRPY)— as the lead candidate for further development, based on its potent broad-spectrum antimicrobial activity and minimal hemolytic effect. TRPY (3 056.908 g/mol) carries the primary sequence RKIIKKWKWKWKKKWWKIWWK-PEG2 (Figure 1B) and exhibits a distinct amphipathic architecture, with cationic lysine (K)/arginine (R) residues clustered along one face and hydrophobic tryptophan residues aligned on the opposite face (Figure 1C), creating an ideal framework for both antimicrobial activity and self-assembly (Deslouches et al., 2005; Liu et al.,

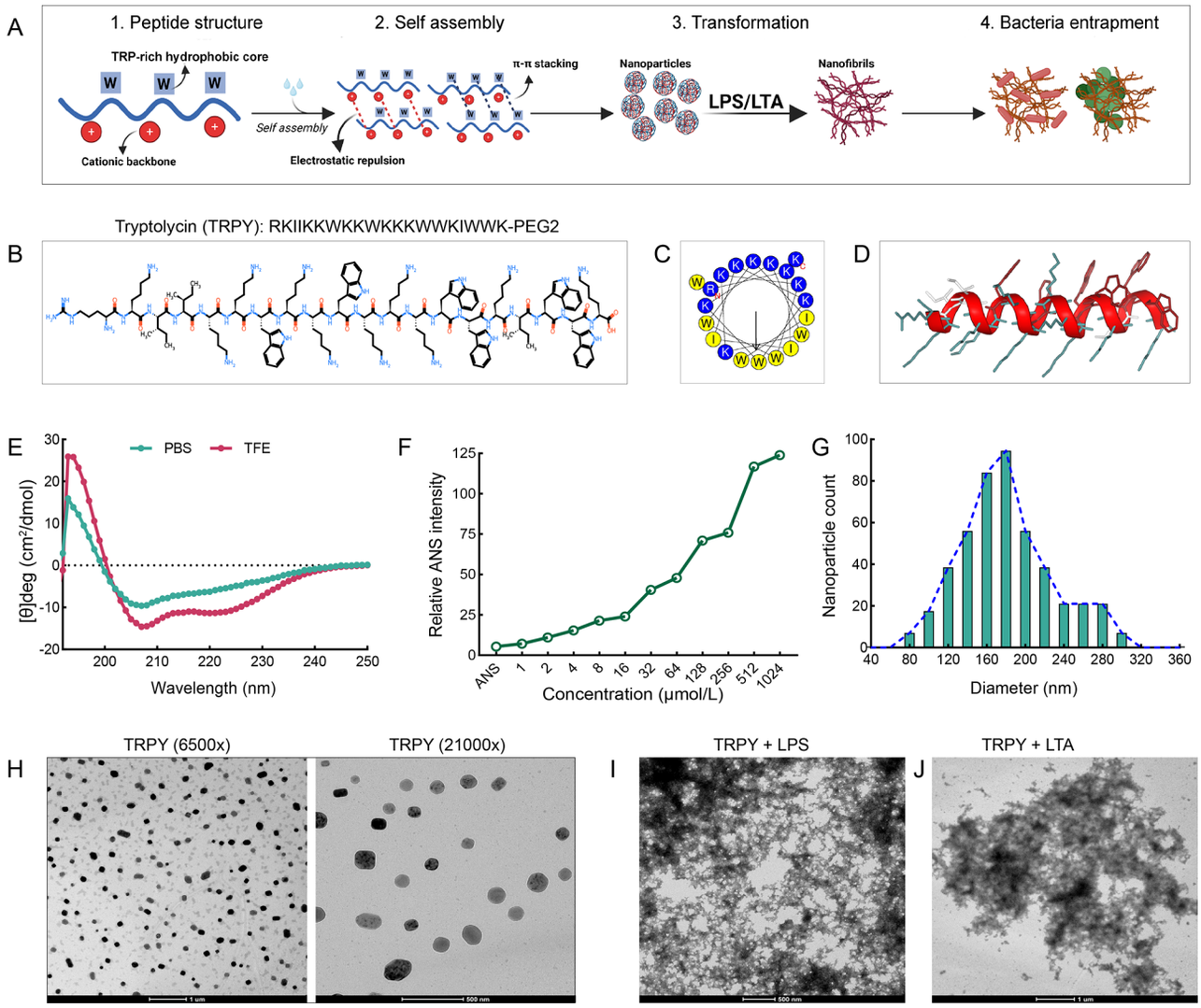

Figure 1 Structural characterization and antimicrobial activity of Tryptolycin (TRPY)

A: Schematic representation of TRPY self-assembly. B: Chemical structure and amino-acid sequence of TRPY. C: Helical wheel projection of TRPY generated with HeliQuest, highlighting amphipathicity with hydrophobic (yellow) and cationic residues (blue) segregated around the helical axis. D: Predicted α-helical secondary structure of TRPY modeled using PEPfold4, illustrating its propensity to adopt a stable α-helical conformation. E: Circular dichroism spectra of TRPY (100 μg/mL) in PBS and 30% TFE, indicating environment-dependent secondary structure. F: Critical aggregation concentration of TRPY. G: Size distribution of TRPY self-assembled nanostructures. H: TEM images of TRPY (100 μmol/L in PBS pH 7.4) at 6 800× (left) and 21 000× (right) magnifications (scale bars: 1 μm and 500 nm, respectively). I: TEM image of TRPY (100 μmol/L) in the presence of 10% *K. pneumoniae* LPS. J: TEM image of TRPY (100 μmol/L) in presence of 10% LTA.

2015). The lysine/arginine-rich motif confers a strong positive charge (+9 at physiological pH), enabling selective electrostatic interactions with negatively charged bacterial membranes and promoting membrane destabilization through carpeting or pore-forming mechanisms (Armstrong et al., 2016; Mollica et al., 2018). Concurrently, the high density of tryptophan residues (8 W in 21 residues) drive π-π stacking and hydrophobic self-assembly, forming stable nanostructures that enhance membrane penetration and biofilm disruption (Khemaissa et al., 2022). Molecular modeling (Figure 1D) confirmed that TRPY adopts a predominantly α-helical conformation, with tryptophan residues forming a contiguous hydrophobic surface that facilitates intermolecular interactions. A small PEG spacer (145 Da) was strategically incorporated at the C-terminus to improve aqueous solubility and proteolytic resistance while preserving antimicrobial potency (Yu et al., 2021).

Structural characteristics of TRPY

Circular dichroism (CD) spectroscopy revealed environment-dependent conformational plasticity in TRPY (Figure 1E). In membrane-mimicking solvent trifluoroethanol (TFE, 30% v/v), TRPY adopted a well-defined α-helical secondary structure, characterized by canonical double minima at 208 nm (π→π* transition) and 222 nm (n→π* transition). In contrast, in aqueous PBS (pH 7.4), the peptide displayed a predominantly random or disordered coil structure, indicating conformational flexibility under non-membranous conditions.

TRPY self-assembles into nanoparticles

Self-assembly behavior was assessed using 8-anilino-1-naphthalenesulfonic acid (ANS) fluorescence, which increases upon binding to hydrophobic domains formed during peptide aggregation. A concentration-dependent enhancement in ANS fluorescence intensity was observed (Figure 1F), with a sharp rise near 4 μg/mL, corresponding to the critical aggregation

concentration (CAC). This relatively low CAC suggests a high propensity for self-assembly, potentially driven by π-π stacking and hydrophobic interactions among clustered tryptophan residues. Dynamic light scattering analysis (Figure 1G) showed that TRPY formed monodisperse nanoparticles with diameters predominantly in the 120–240 nm range and an average size of approximately 160 nm. TEM imaging (Figure 1H) confirmed the formation of spherical nanoparticles with well-defined morphology. These results illustrate one of the few documented instances in which an AMP assembles into discrete, spherical nanoparticles rather than the fibrillar structures commonly associated with amyloidogenic sequences (Chou et al., 2023; Lai et al., 2021). Notably, in the presence of bacterial cell wall components—LTA and LPS—TRPY nanoparticles transformed into fibrous structures (Figure 1I, J), indicating structural adaptability in response to environmental signals. This transition is consistent with previous studies showing AMP oligomerization upon interaction with LTA or LPS from Gram-positive and Gram-negative bacteria, respectively (Ma et al., 2024). To assess the functional significance of this structural transformation, bacterial aggregation assays were conducted. TRPY was incubated with *K. pneumoniae* and MRSA at concentrations ranging from 10 to 80 μmol/L for 4 h at 37°C. A dose-dependent formation of visible precipitates was observed for both strains (Supplementary Figure S2), confirming that the fibrillar network formation directly translates to effective bacterial immobilization.

TRPY exhibits potent antimicrobial activity against multidrug-resistant bacteria

TRPY exhibited robust broad-spectrum antimicrobial activity against a range of clinically relevant bacterial species, including *Escherichia coli* and the notoriously challenging ESKAPE pathogens (*Enterococcus faecium*, *Staphylococcus aureus*, *Klebsiella pneumoniae*, *Acinetobacter baumannii*, and *Pseudomonas aeruginosa*), which are responsible for most global nosocomial infections (Miller & Arias, 2024) (Figure 2A). The MICs across these species ranged from 0.3 to 1.0 μmol/L, with minimal difference between the MIC and minimum bactericidal concentration (MBC), indicating a predominantly bactericidal rather than a bacteriostatic mode of action. Against clinical isolates of multidrug-resistant *K. pneumoniae* (Figure 2B), TRPY maintained excellent antimicrobial efficacy across all strains, with MICs ranging from 0.5 to 1.0 μmol/L. Notably, TRPY maintained full antimicrobial activity against colistin-resistant and gentamicin-resistant strains, with some isolates showing resistance to gentamicin at concentrations greater than 128 μmol/L but remaining fully susceptible to TRPY. Similar efficacy was observed in clinical MRSA isolates (Figure 2C), with TRPY displaying MICs between 0.39 and 1.0 μmol/L and outperforming vancomycin and gentamicin in multiple strains.

TRPY resists proteolytic degradation and remains stable under physiological conditions

One of the principal barriers to clinical translation of AMPs is their susceptibility to rapid proteolytic degradation by proteolytic enzymes, reduced efficacy under high-salt physiological conditions, and off-target cytotoxicity to mammalian cells (Mwangi et al., 2023; Wang et al., 2019). TRPY exhibited moderate resistance to proteolysis, a critical property for survival in environments rich in host enzymes. Notably, the peptide retained 80% integrity after 30 min of

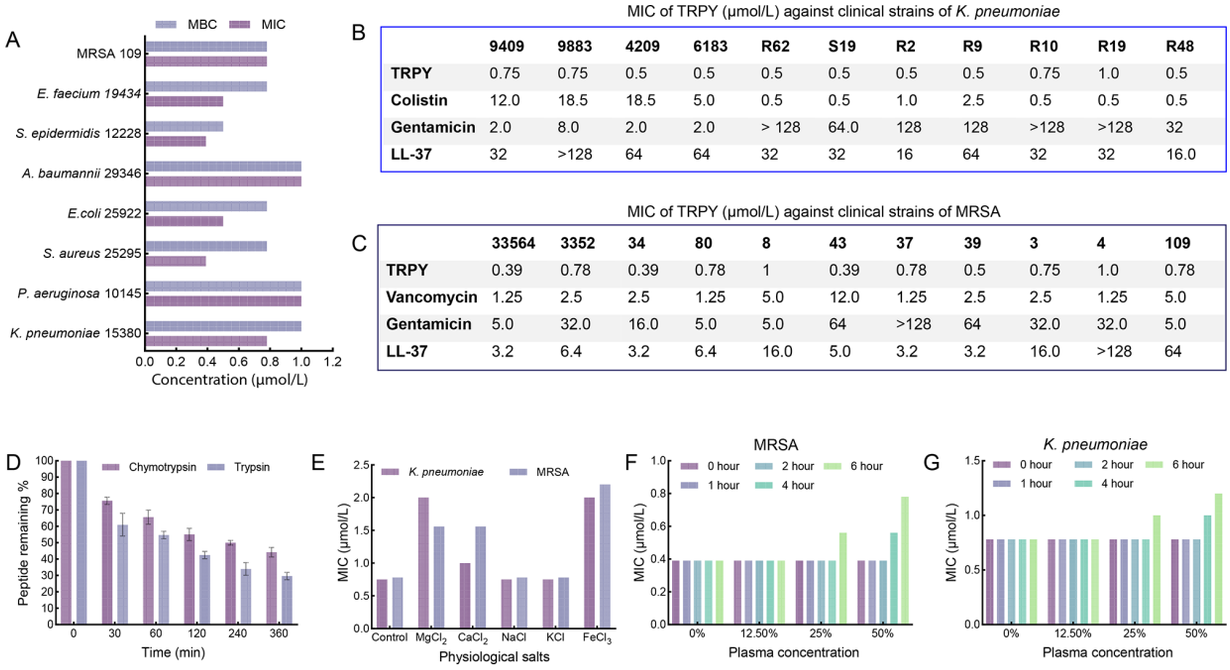

	9409	9883	4209	6183	R62	S19	R2	R9	R10	R19	R48
TRPY	0.75	0.75	0.5	0.5	0.5	0.5	0.5	0.5	0.75	1.0	0.5
Colistin	12.0	18.5	18.5	5.0	0.5	0.5	1.0	2.5	0.5	0.5	0.5
Gentamicin	2.0	8.0	2.0	2.0	> 128	64.0	128	128	>128	>128	32
LL-37	32	>128	64	64	32	32	16	64	32	32	16.0

	33564	3352	34	80	8	43	37	39	3	4	109
TRPY	0.39	0.78	0.39	0.78	1	0.39	0.78	0.5	0.75	1.0	0.78
Vancomycin	1.25	2.5	2.5	1.25	5.0	12.0	1.25	2.5	2.5	1.25	5.0
Gentamicin	5.0	32.0	16.0	5.0	5.0	64	>128	64	32.0	32.0	5.0
LL-37	3.2	6.4	3.2	6.4	16.0	5.0	3.2	3.2	16.0	>128	64

Figure 2 Antimicrobial activity and physiological stability of TRPY

A: MIC and MBC values of TRPY against representative nosocomial pathogens. B: Comparison of MICs (μmol/L) among TRPY, colistin, gentamicin, and LL-37 against clinical strains of *K. pneumoniae*. C: Comparison of MICs (μmol/L) among TRPY, vancomycin, gentamicin, and LL-37 against clinical strains of methicillin-resistant *S. aureus* (MRSA). D: Proteolytic stability of TRPY following incubation with chymotrypsin and trypsin over 6 h, showing percentage of intact peptide remaining, as determined by RP-HPLC. E: Influence of physiological salts (150 mM) on MICs of TRPY against *K. pneumoniae* and MRSA. F, G: Effect of plasma on antimicrobial activity of TRPY against MRSA and *K. pneumoniae*, respectively, showing MICs after incubation with different concentrations of plasma (0%, 12.5%, 25%, and 50%) for various durations. Data are presented as mean±SEM from three independent experiments.

exposure to chymotrypsin or trypsin (peptide: enzyme 50:1), with degradation progressing to 60%–70% at 60 min, 50%–60% at 120 min, and 30%–40% after 360 min (Figure 2D). This gradual degradation profile supports the potential for sustained *in vivo* activity and compares favorably to many natural peptides, such as LL-37, which are often rapidly degraded (within 1 h) by plasma enzymes (Sieprawska-Lupa et al., 2004).

The sensitivity of many AMPs to physiological salt concentrations represents another significant barrier to therapeutic development, as divalent and trivalent cations are particularly disruptive to AMP function via competitive displacement from bacterial membranes (Chu et al., 2013; Yao et al., 2023). As shown in Figure 2E, various physiological salts (150 mmol/L) exerted differential effects on the antimicrobial activity of TRPY against *K. pneumoniae* and MRSA. $FeCl_3$ and $MgCl_2$ produced the most pronounced inhibitory effects, increasing MICs to approximately 2.0 μmol/L for both pathogens. In contrast, KCl, NaCl, and $CaCl_2$ caused minimal interference with antimicrobial activity. The preserved efficacy in the presence of monovalent cations suggests that TRPY remains active under physiologically relevant ionic conditions, addressing a critical limitation that has hindered the clinical development of many AMPs.

TRPY is stable in physiological fluids

Loss of antimicrobial efficacy in biological fluids is a significant bottleneck in the development of peptide-based therapeutics, primarily due to protein binding and ionic interference. As shown in Figure 2F, G, TRPY maintained potent activity against both *K. pneumoniae* 9409 and MRSA 33564 across increasing plasma concentrations (0%, 12.5%, 25%, and 50%) over the 6 h incubation period. MIC values against *K. pneumoniae* remained consistently below 1.0 μmol/L, with only minor elevation observed at 6 h in 50% plasma. Similarly, against MRSA, MICs remained below 0.8 μmol/L across all tested conditions. These findings indicate that TRPY retains functional stability and antimicrobial potency in plasma, strongly supporting its potential for clinical applications.

TRPY exhibits minimal cytotoxicity toward mammalian cells

Cytotoxicity to host cells poses one of the most significant obstacles to the clinical advancement of AMPs (Lei et al., 2019). As shown in Figure 3A, TRPY induced less than 10% hemolysis even at the highest tested concentration, markedly lower than that observed for magainin 2 and LL-37, indicating strong selectivity for microbial over mammalian membranes. Further cytotoxicity assays performed on HaCaT keratinocytes, RAW264.7 macrophages, and HEK293 kidney cells confirmed this selectivity (Figure 3B, C). A consistent pattern emerged across all cell types, with magainin 2 exhibiting significant dose-dependent cytotoxicity, reducing cell viability to below 20% at concentrations above 40 μmol/L. In contrast, TRPY maintained over 80% cell viability across nearly all concentrations and cell types. This combination of potent antimicrobial activity with minimal mammalian toxicity represents an ideal safety profile for therapeutic development.

TRPY exhibits limited *in vivo* toxicity

Minimizing host toxicity remains a key priority in the development of new antimicrobial agents to address the global crisis of antimicrobial resistance. To assess the *in vivo* toxicity profile of TRPY, intraperitoneal administration was performed in mice over a 5 day period at doses of 5 and 10 mg/kg, with PBS as the control. Body weight measurements (Supplementary Figure S3A) revealed stable weights across all groups, with no significant differences between the TRPY-treated and control groups, indicating the absence of systemic toxicity typically associated with weight loss. Liver function biomarkers (Supplementary Figure S3B) showed that alanine aminotransferase (ALT) and aspartate aminotransferase (AST) levels remained within physiological ranges across all treatment groups. Mean ALT values were 22.9±1.7 U/L, 22.8±2.6 U/L, and 23.4±3.2 U/L in the PBS, 5 mg/kg, and 10 mg/kg groups, respectively, while AST levels were 101.3±5.4 U/L, 102.7±6.6 U/L, and 105.2±4.7 U/L, respectively, indicating no evidence of hepatocellular injury. Renal function parameters, including serum urea and alkaline phosphatases (ALP) levels, were also comparable across treatment groups. Serum urea concentrations were 11.5±1.1 μmol/L, 11.2±1.5 μmol/L, and 12.1±1.2 μmol/L in the PBS, 5 mg/kg, and 10 mg/kg groups, respectively, indicating that renal function remains intact following TRPY exposure. These findings are notable given the nephrotoxic and hepatotoxic liabilities that limit the clinical utility of many AMPs and last-line antibiotics, such as colistin (Jafari & Elyasi, 2021). Histopathological examination of critical organs, such as the liver and kidney (Supplementary Figure S3C), corroborated the biochemical data. Liver sections displayed normal architecture with well-preserved hepatocyte morphology and no signs of necrosis, inflammation, or fatty degeneration. Similarly, kidney sections exhibited normal glomerular and tubular architecture, with well-preserved glomerular capsules and no tubular dilatation, protein casts, or interstitial inflammation suggestive of nephrotoxicity. Collectively, these results indicate that TRPY administration at therapeutically relevant doses induces negligible toxicity *in vivo*, supporting its advancement as a safe antimicrobial candidate for further investigation and preclinical development.

***In vivo* pharmacokinetics of TRPY in mice**

To evaluate systemic stability and clearance kinetics, pharmacokinetic profiling of TRPY was performed in mice following a single intravenous injection at 5 mg/kg. Plasma concentrations were quantified over an 8 h period using HPLC analysis. As shown in Supplementary Figure S4, TRPY exhibited a biphasic elimination profile. An initial rapid distribution phase was observed within the first 2 h, with plasma levels decreasing from approximately 15 000 ng/mL at 0.25 h to below 1 000 ng/mL by 2 h post-injection. This was followed by a slower elimination phase, with plasma concentrations declining to approximately 120 ng/mL at 8 h. The pharmacokinetic profile suggests that TRPY undergoes rapid initial distribution followed by sustained systemic clearance. The persistence of quantifiable peptide levels throughout the 8 h timeframe reflects favorable *in vivo* stability and supports the potential of TRPY for systemic therapeutic application.

TRPY exhibits rapid and potent bactericidal activity

Time-kill kinetics were used to characterize the bactericidal efficacy and speed of TRPY (Hossain, 2024). At 2 μmol/L, TRPY eradicated all viable MRSA 33565 cells within 60 min, significantly outperforming gentamicin (20 μmol/L), which required over 360 min to achieve comparable results (Figure 4A). Similarly, 2 μmol/L TRPY eliminated all viable *K. pneumoniae* 9409 cells within 60 min, whereas gentamicin at

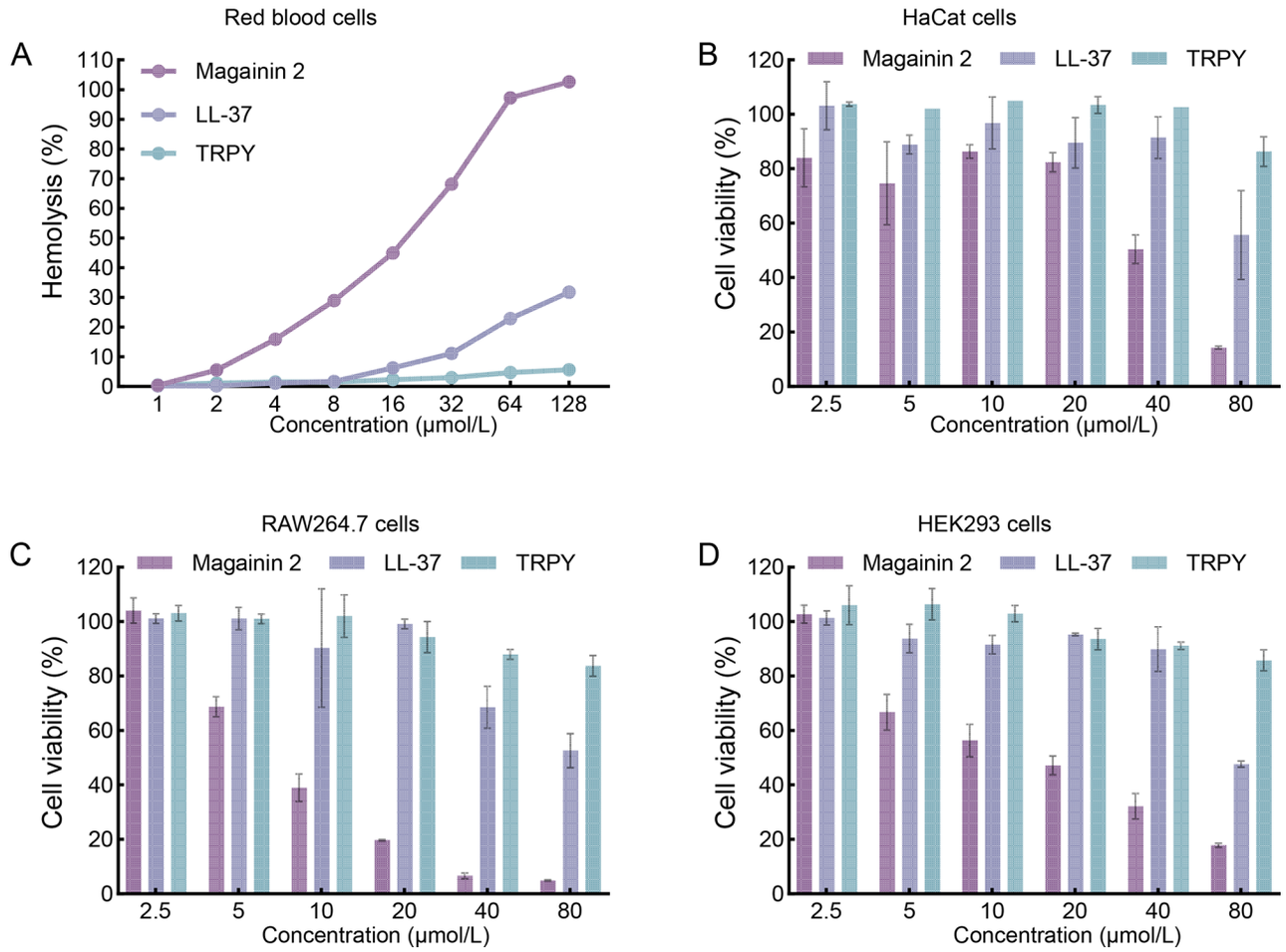

Figure 3 Cytotoxicity profile of Tryptolycin (TRPY)

A: Hemolytic activity of TRPY compared to LL-37 and magainin 2 against mouse red blood cells, showing minimal hemolysis by TRPY even at high concentrations. B, C: Cytotoxic effects of TRPY, LL-37, and magainin 2 against mammalian cell lines, including HaCaT (human keratinocytes), RAW264.7 (murine macrophages), and HEK293 (human embryonic kidney cells). Cell viability was determined using the CCK8 assay after 24 h of treatment with varying peptide concentrations (2.5–80 μmol/L). Data are presented as mean±SEM from three independent experiments.

10-fold higher concentration (20 μmol/L) produced only partial killing over the same time period. This stark contrast in potency and speed suggests a mechanism of action distinct from conventional antibiotics, likely targeting essential structural components rather than interference with metabolic pathways, which typically require prolonged exposure to induce cell death (Harms et al., 2016). Bacterial spotting assays further corroborated the bactericidal activity of TRPY, showing complete growth inhibition at concentrations ≥1 μmol/L for both pathogens (Figure 4B), and no regrowth occurred even after extended incubation, indicating irreversible bactericidal effects rather than temporary inhibition.

TRPY exerts bactericidal activity through rapid membrane interaction and destabilization

To elucidate the mechanism underlying the bactericidal activity, a series of complementary assays were employed. Results consistently supported membrane disruption as the primary mode of action (Selvarajan et al., 2023).

Membrane permeabilization assays (outer and cytoplasmic membranes)

Disruption of bacterial membranes by TRPY was evaluated using complementary fluorescence-based assays. The N-phenyl-1-naphthylamine (NPN) uptake assay (Figure 4C) revealed that TRPY effectively permeabilized the outer membrane of *K. pneumoniae* in a dose-dependent manner. NPN, a hydrophobic fluorescent probe that increases fluorescence intensity upon insertion into a phospholipid environment (Selvarajan et al., 2023), exhibited enhanced fluorescence intensity after TRPY treatment compared to untreated controls, indicating disrupted outer membrane integrity, a critical barrier in Gram-negative bacteria. Consistently, the PI uptake assay (Figure 4D) confirmed cytoplasmic membrane disruption in both MRSA and *K. pneumoniae*. TRPY exposure induced a concentration-dependent increase in PI fluorescence, indicating loss of cytoplasmic membrane integrity and corresponding cell death. Notably, TRPY induced greater membrane permeability than established membrane-active antibiotics vancomycin (for MRSA) and colistin (for *K. pneumoniae*).

Fluorescence microscopy analysis of membrane damage

Fluorescence microscopy using SYTOX Green and PI double staining further visualized TRPY-mediated membrane damage (Figure 4E). In untreated samples, bacteria exhibited strong SYTOX Green fluorescence with minimal PI staining, consistent with intact membranes and cell viability. In contrast, treatment with 2 μmol/L TRPY induced substantial PI uptake (red signal) in both MRSA and K. *pneumoniae*, indicating

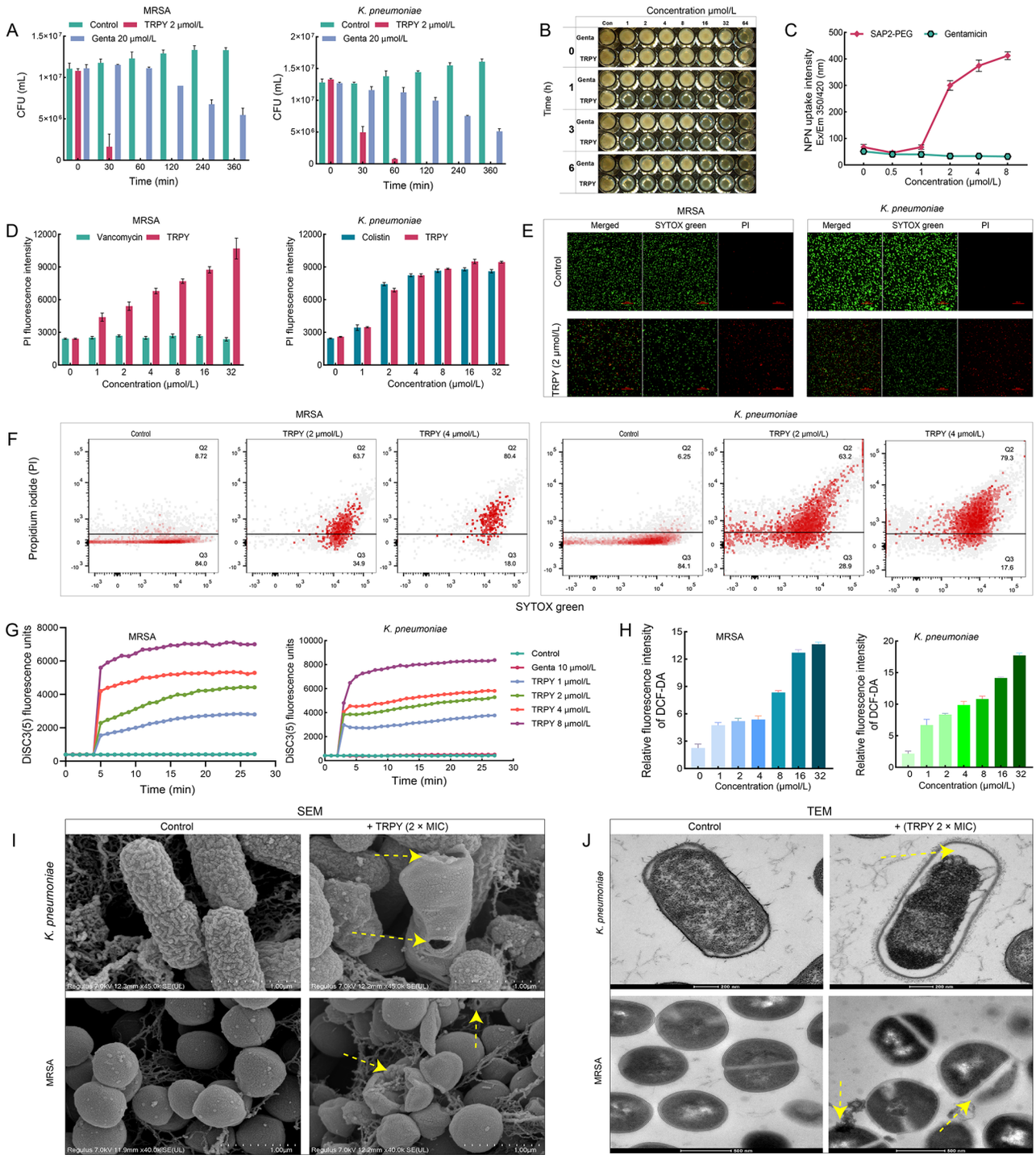

Figure 4 Mechanism of action of Tryptolycin (TRPY) against microbial cells

A: Time-kill kinetics of TRPY against MRSA (left) and *K. pneumoniae* (right). B: Agar spotting assay showing concentration-dependent bacterial killing. C: Outer membrane permeabilization of *K. pneumoniae* assessed by NPN uptake. D: Membrane permeabilization assessed by propidium iodide (PI) fluorescence intensity. E: Fluorescence microscopy images of MRSA and *K. pneumoniae* treated with TRPY showing effects on membrane integrity. Untreated controls (top) and TRPY-treated (2 μmol/L, bottom) bacteria visualized with merged channels, SYTOX green (membrane permeability), and PI (dead cell indicator). F: Flow cytometry dot plots showing PI uptake in control versus TRPY-treated (2 μmol/L and 4 μmol/L) bacteria. G: Inner membrane depolarization using $DiSC_3(5)$ fluorescence measurement. H: Dose-dependent DC-FDA fluorescence intensity showing ROS generation in MRSA and *K. pneumoniae* after TRPY treatment. I: SEM images of *K. pneumoniae* and MRSA control versus TRPY-treated (2× MIC) bacteria. Yellow arrows indicate membrane damage and morphological changes in treated cells. J: TEM images of *K. pneumoniae* and MRSA control versus TRPY-treated (2× MIC) bacteria. Yellow arrows indicate cytoplasmic damage and membrane disruption in treated cells. Data points represent mean±SEM from three independent experiments.

membrane permeabilization sufficient to allow entry of the normally excluded membrane-impermeable nucleic acid dye. Merged images revealed transformation from a colony dominated by survival (green) under control conditions to a

mixed colony containing cells with impaired membrane integrity after TRPY treatment, confirming progressive disruption of membrane integrity and loss of viability.

Flow cytometry quantification of membrane damage

Flow cytometry provided quantitative validation of membrane permeabilization (Figure 4F). Following TRPY treatment (4 μmol/L), the proportion of PI-positive cells increased from 0.72% to 83.7% in MRSA and from 0.2% to 79.3% in *K. pneumoniae*. Most of the bacterial population shifted into the PI-positive quadrant (Q2), confirming that TRPY induced extensive membrane damage across the population. These findings corroborate the rapid bactericidal activity observed in the time-kill assays and support a membrane-targeting mode of action.

TRPY induces rapid membrane depolarization

Membrane potential disruption by TRPY was evaluated using the membrane potential-sensitive probe $DiSC_3(5)$ (Figure 4G). Following TRPY treatment, both *K. pneumoniae* and MRSA exhibited a sharp increase in fluorescence within 5 min, indicating rapid dissipation of membrane potential. This was followed by a gradual increase over the 30 min observation period. In contrast, untreated controls and gentamicin-treated samples maintained baseline fluorescence, consistent with intact membrane potential. This rapid depolarization profile precedes and likely contributes to the membrane permeabilization and bactericidal effects observed in the other assays.

TRPY induces intracellular oxidative stress

In addition to direct membrane disruption, TRPY also induced concentration-dependent ROS generation, as assessed by DCFDA fluorescence intensity (Figure 4H). Both MRSA and *K. pneumoniae* displayed progressively elevated ROS levels with increasing TRPY concentrations, suggesting that oxidative stress may complement TRPY-mediated membrane disruption by contributing to intracellular damage and amplifying bactericidal activity.

Ultrastructural evidence of membrane damage

SEM and TEM provided compelling visual evidence of TRPY-induced structural damage (Figure 4I, J). SEM images revealed pronounced surface deformation, membrane rupture, and cellular collapse in both pathogens following treatment at 2× MIC. TEM analysis further showed discontinuities in the membrane, cytoplasmic leakage, and intracellular disorganization (indicated by yellow arrows). These ultrastructural alterations are consistent with the functional membrane disruption detected in the fluorescence-based assays, confirming the membrane-targeting action of TRPY across both Gram-positive and Gram-negative species and representing a significant advantage over traditional antibiotics limited due to structural differences in bacterial cell envelopes.

TRPY potentially interacts with microbial DNA

In addition to membrane and oxidative damage, gel electrophoresis revealed that TRPY at concentrations ≥4 μmol/L induced degradation or binding to bacterial DNA (Supplementary Figure S5). This observation suggests a potential secondary mechanism involving DNA interaction, which may enhance bacterial killing efficacy and reduce the likelihood of resistance development.

TRPY exhibits potent antibiofilm and antipersister activity

Both *K. pneumoniae* and MRSA are well known for their capacity to form biofilms and generate persister cells, contributing to persistent and recurrent infections in clinical settings (Niu et al., 2024). Notably, *K. pneumoniae* biofilms are frequently implicated in ventilator-associated pneumonia, urinary tract infections, and catheter-related bloodstream infections (Chung, 2016), while MRSA biofilms are commonly associated with chronic wound infections, osteomyelitis, and endocarditis (Craft et al., 2019). These infections are notoriously difficult to treat, as conventional antibiotics are often ineffective against biofilm-embedded infections, highlighting the urgent need for novel therapeutic agents that target biofilms and persisters.

TRPY significantly inhibited biofilm formation by both pathogens in a concentration-dependent manner (Figure 5A, B). Marked inhibition was observed at concentrations as low as 2 μmol/L, with near-complete inhibition (approximately 95% reduction compared to control) achieved at 32 μmol/L. This suggests that TRPY interferes with initial attachment and subsequent colonization. In addition to preventing biofilm establishment, TRPY effectively eradicated preformed biofilms of *K. pneumoniae* and MRSA (Figure 5C, D), achieving over 40% biofilm reduction at just 8 μmol/L. This ability to disrupt mature biofilms is particularly important given the protective barrier function of the extracellular polymeric substance (EPS) matrix and the altered metabolic states of embedded bacteria that typically limit antibiotic penetration and efficacy (Singh et al., 2021).

Importantly, TRPY also exhibited potent activity against persister populations of both bacterial species (Figure 5E, F). In *K. pneumoniae*, TRPY at 0.5× MIC significantly reduced CFU/mL from 6.2×10^6 in the control to virtually undetectable levels at 8× MIC. Similarly, in MRSA, TRPY induced substantial reduction at 0.5× MIC, with complete eradication at 8 μmol/L. These results highlight the ability of TRPY to eliminate drug-tolerant persisters, a critical barrier in the treatment of chronic and relapsing infections.

TRPY binds to and disrupts the supramolecular structure of LPS

LPS, a major constituent of the Gram-negative bacterial outer membrane, plays an essential role in pathogenicity and serves as a key target for antimicrobial drug development (Jan, 2017). It also functions as a potent endotoxin, activating host pattern recognition receptors and triggering inflammatory responses that contribute to sepsis and other severe inflammatory conditions (Cavaillon, 2018; Mazgaeen & Gurung, 2020). Therapeutics capable of both neutralizing LPS and exerting intracellular antimicrobial activity hold considerable promise for the treatment of complex bacterial infections.

TRPY-LPS interaction and inhibition of LPS-induced cytokine production were evaluated using the BODIPY-TR-cadaverine displacement assay, which measures the ability of compounds to displace fluorescent probes from LPS complexes. As shown in Figure 6A, TRPY demonstrated strong, concentration-dependent binding to LPS, with a displacement profile comparable to polymyxin B (PMB) and LL-37, two well-characterized LPS-binding AMPs. These results indicate that TRPY can directly interact with and potentially neutralize LPS under infectious conditions. A similar displacement pattern was observed for LTA, indicating that TRPY can also effectively bind to LTA (Supplementary Figure S6).

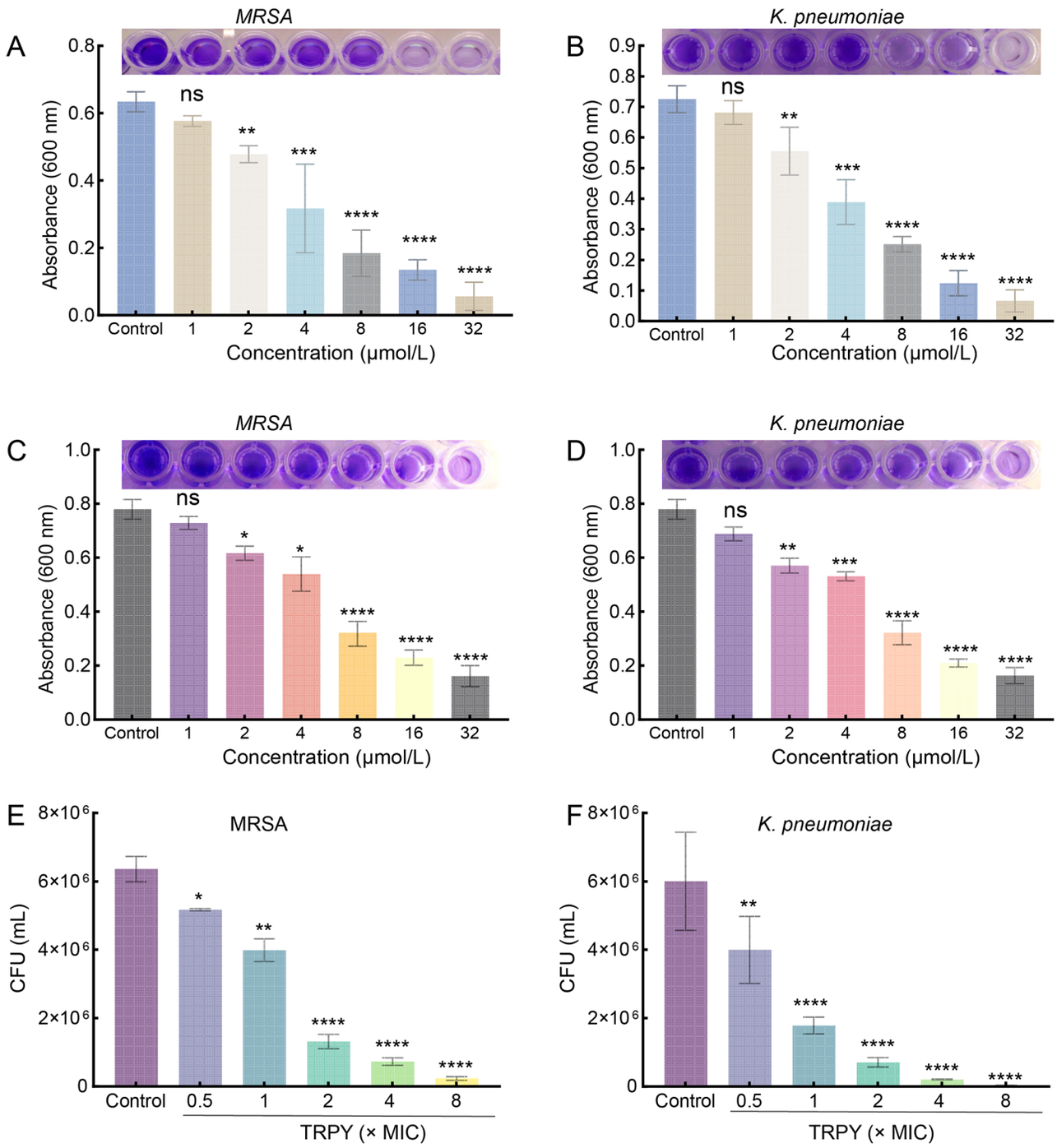

Figure 5 Effects of Tryptolycin (TRPY) on *K. pneumoniae* and MRSA biofilms and persister cells

A, B: Dose-dependent inhibition of MRSA and *K. pneumoniae* biofilm formation, respectively. Biofilm formation was quantified by measuring absorbance at 600 nm. Top inserts are representative 96-well plate images of biofilms stained with 0.1% crystal violet. C, D: Eradication of pre-formed MRSA and *K. pneumoniae* biofilms. Remaining biofilm was quantified by measuring absorbance at 600 nm. E, F: Elimination of MRSA and *K. pneumoniae* persister cells following 1 h of incubation with increasing TRPY concentrations. For all panels, Control represents untreated control. Error bars indicate SEM. Statistical significance compared to control is denoted as: ns: Not significant; *: P<0.05; **: P<0.01; ***: P<0.001; ****: P<0.0001.

TEM was further employed to visualize the effects of TRPY on LPS supramolecular structure (Figure 6B). Results indicated that LPS alone formed ribbon-like supramolecular structures with uniform density and organization. In contrast, TRPY treatment disrupted this organized structure, yielding amorphous aggregates with irregular morphology and increased electron density. These morphological alterations suggest that TRPY interacts directly with LPS molecules, disrupting the intermolecular forces that maintain their supramolecular organization.

TRPY reduces intracellular bacterial load and LPS-induced cytokine production in mouse macrophages

The intracellular antibacterial activity of TRPY was assessed using RAW264.7 macrophages, a model system for studying host-pathogen interactions. As depicted in Figure 6C,

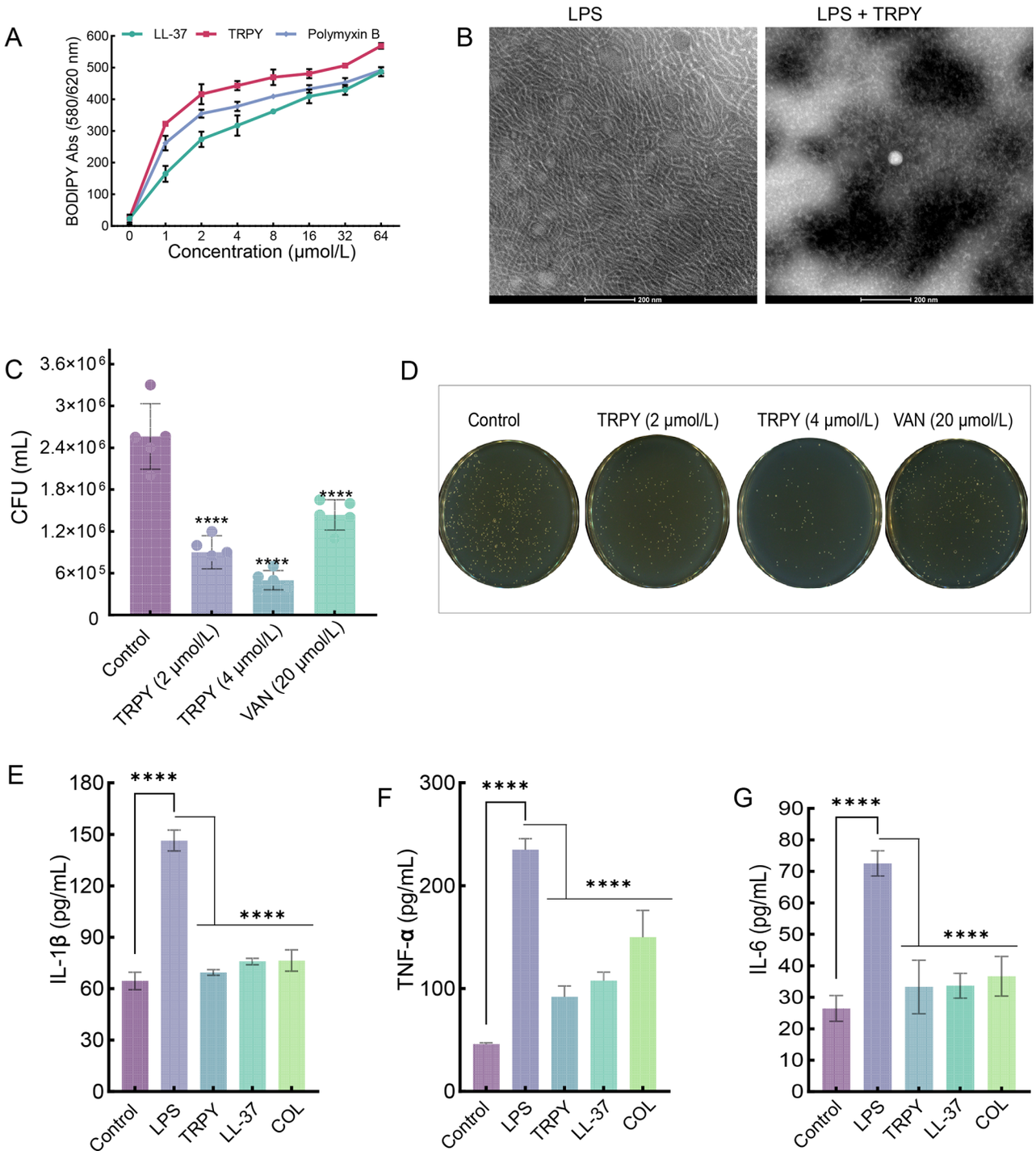

Figure 6 Intracellular antibacterial activity and inhibition of LPS-induced inflammatory responses

A: LPS binding affinity measured by BODIPY displacement assay. B: TEM images (scale bar: 200 nm) showing the effect of Tryptolycin (TRPY) on LPS supramolecular structure. C: Intracellular antibacterial activity against MRSA-infected RAW264.7 macrophages (compared to control ****: P<0.0001). D: Representative images of bacterial colony growth on agar plates corresponding to treatments in panel C, showing apparent reduction in colonies under TRPY treatment at 2 μmol/L and 4 μmol/L compared to control. E–G: Inhibition of LPS-induced pro-inflammatory cytokine production in RAW264.7 cells. VAN represents vancomycin, and COL represents colistin. Statistical significance compared with LPS-only group, ****: P<0.0001.

treatment with 2 μmol/L and 4 μmol/L TRPY reduced intracellular bacterial burden from approximately 2.5×10^5 CFU/mL in the untreated control to 1.0×10^5 and 0.5×10^5 CFU/mL, respectively (P<0.0001). At 4 μmol/L, TRPY outperformed vancomycin (20 μmol/L), which yielded approximately 1.5×10^5 CFU/mL. These findings were visually corroborated by colony formation assays (Figure 6D), which showed a clear concentration-dependent reduction in bacterial colonies following TRPY treatment, with 4 μmol/L TRPY demonstrating equivalent or superior efficacy relative to vancomycin.

Modulation of host inflammatory responses also represents an important attribute for antimicrobial agents, particularly in the context of severe infections where excessive inflammation

contributes to pathology. Results showed that TRPY modulated the inflammatory response in LPS-stimulated RAW264.7 macrophages. As shown in Figure 6E–G, LPS stimulation significantly increased the secretion of IL-1β, TNF-α, and IL-6 compared to unstimulated controls (P<0.0001). TRPY treatment effectively attenuated these cytokine levels in a concentration-dependent manner, reducing IL-1β, TNF-α, and IL-6 to approximately 90, 70, and 33 pg/mL, respectively, compared to 230, 145, and 72 pg/mL in LPS-only controls. This immunomodulatory effect was comparable to that observed with LL-37 and colistin, two reference AMPs with established anti-inflammatory properties. The dual ability of TRPY to eliminate intracellular pathogens and attenuate pro-inflammatory cytokine production supports its potential utility in treating infections characterized by both microbial persistence and excessive inflammation.

Efficacy of TRPY in *K. pneumoniae* acute pulmonary infection

Klebsiella pneumoniae lung infections are characterized by rapid tissue destruction and inflammation mediated by potent virulence factors (Russo & Marr, 2019). A prominent feature is the polysaccharide capsule, which impairs phagocytosis and complement-mediated clearance, facilitating extensive bacterial proliferation and resulting in necrotizing pneumonia, hemorrhagic alveolar injury, and abscess formation (Ernst et al., 2020; Ko, 2017). In murine models, encapsulated strains invade lung epithelial cells and trigger robust neutrophil recruitment and cytokine release, paradoxically exacerbating tissue damage (Russo & Marr, 2019). Using female CD-1 mice (8–10 weeks old, 25–30 g), the efficacy of TRPY was assessed in an acute pulmonary infection model (Figure 7A). Treatment with 2 mg/kg TRPY significantly reduced pulmonary bacterial burden by approximately 1 log compared to the control group, exhibiting comparable efficacy to colistin at the same dose (Figure 7B). TRPY also markedly attenuated the inflammatory response elicited by *K. pneumoniae* infection (Figure 7C). Cytokine profiling revealed substantial reductions in MCP-1 (58.4%), IL-6 (39.2%), TNF-α (34.7%), and IL-1β (42.8%) compared with the control group.

Histological examination of lung tissue (Figure 7D) further corroborated these findings. The vehicle group exhibited severe lung inflammation, characterized by alveolar congestion, neutrophilic infiltration, and interstitial edema. In contrast, TRPY-treated mice displayed a significant improvement in lung structure, characterized by reduced inflammatory cell infiltration and preserved alveolar architecture. Compared to the vehicle group, lung tissue from TRPY-treated mice more closely resembled that of healthy controls and showed slightly improved histological features compared to colistin-treated mice.

Efficacy of TRPY in an MRSA peritoneal infection model

To evaluate the *in vivo* efficacy of TRPY against Gram-positive pathogens, a peritoneal infection model was established in CD-1 mice using MRSA 33564 (1×10^8 CFU/mL). Intraperitoneal administration of 10 mg/kg TRPY significantly reduced bacterial loads across multiple compartments. In peritoneal lavage fluid (Figure 7E), bacterial colony counts decreased from approximately 1×10^8 CFU/mL to 5.5×10^7 CFU/mL (3-fold reduction, P<0.01) compared to vehicle controls. More pronounced reductions were observed in liver and kidney tissues (Figure 7F, G), with bacterial loads reduced by approximately 5-fold and 4-fold, respectively. Histopathological analysis (Figure 7H) revealed that the TRPY-treated group maintained normal tissue architecture in the liver and kidneys, compared with infected animals treated with the vehicle, which showed significant inflammatory changes. These results indicate that TRPY reduced both bacterial dissemination and infection-associated tissue damage.

Efficacy of TRPY in LPS-induced endotoxemia model

Given the critical role of LPS in sepsis, the antiendotoxin properties of TRPY (10 mg/kg) were compared with equivalent doses of LL-37 and colistin in an LPS-induced endotoxemia model. Recognition of LPS by TLR4 triggers macrophage activation, which, in turn, triggers the production of NF-κB-dependent proinflammatory cytokines, ultimately leading to systemic inflammatory potential, septic shock, and death (Chen et al., 2021; Ciesielska et al., 2021) (Figure 7I). Following intraperitoneal LPS administration (10 mg/kg), TRPY treatment significantly attenuated cytokine responses in CD-1 mice (Figure 7J). TRPY treatment reduced IL-6 by 42.3% (P<0.01), MCP-1 by 46.6% (P<0.01), TNF-α by 39.5% (P<0.001), and IL-1β by 52.3% (P<0.01) relative to LPS-only controls. Notably, TRPY showed superior anti-inflammatory efficacy compared with LL-37 and colistin for most measured cytokines, especially the inhibition of TNF-α and IL-1β. The enhanced anti-endotoxin activity of TRPY may stem from its ability to neutralize LPS and disrupt TLR4-mediated signaling cascades, consistent with the previously described mechanism of cationic AMPs (Brandenburg et al., 2016). This dual antimicrobial and immunomodulatory activity underscores the therapeutic potential of TRPY in treating infections complicated by endotoxemia and sepsis.

DISCUSSION AND CONCLUSION

This study presents a promising blueprint in AMP design, successfully addressing multiple limitations that have hindered the clinical translation of AMPs. TRPY integrates a cationic amphipathic backbone with a tryptophan-rich hydrophobic core, creating a unique dual-functionality platform that exhibits potent antimicrobial activity and the capacity for controlled self-assembly into nanostructures. The environment-responsive conformational plasticity of TRPY—transitioning from a disordered state in aqueous media to an α-helical structure upon membrane contact—recapitulates a strategy employed by endogenous AMPs such as LL-37 and magainin, which adopt functional secondary structures upon contact with bacterial membranes (Sancho-Vaello et al., 2020). This adaptive folding minimizes off-target interactions with host cells while enabling rapid structural reorganization at infection sites (Zeth & Sancho-Vaello, 2021). Furthermore, the structural adaptability of TRPY, which transforms from spherical nanoparticles to fibrous structures upon contact with bacterial cell wall components (LPS and LTA), represents a sophisticated pathogen recognition capability that may enhance antimicrobial efficacy through bacterial entrapment, as revealed by concentration-dependent bacterial aggregation experiments.

TRPY exhibited broad-spectrum antimicrobial activity against ESKAPE pathogens, with MICs ranging from 0.3 to 1.0 μmol/L, and maintained efficacy against multidrug-resistant clinical isolates of colistin-resistant *K. pneumoniae* and MRSA. The minimal difference between MIC and MBC values confirmed rapid bactericidal activity, an essential

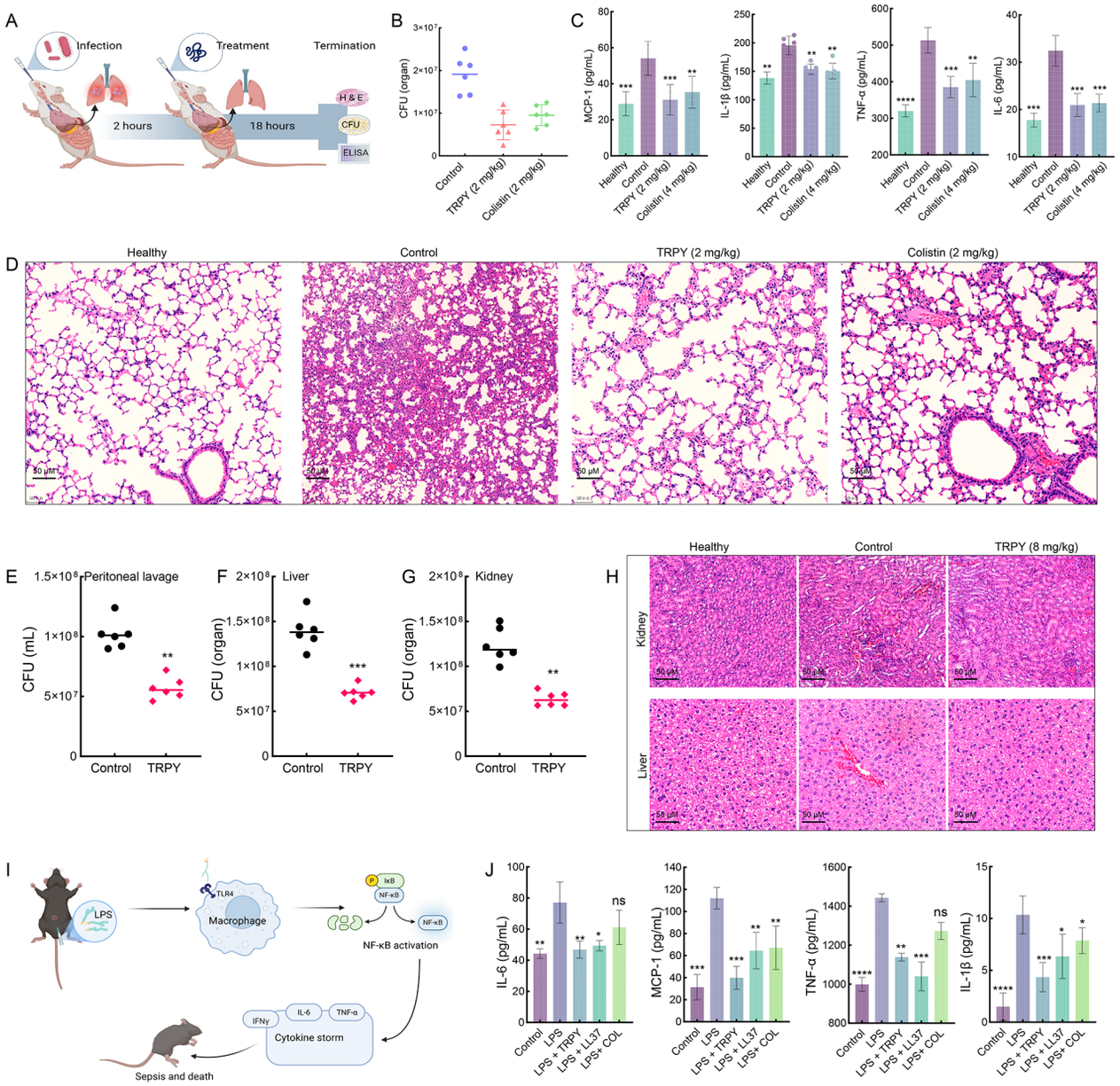

Figure 7 ***In vivo*** **efficacy of Tryptolycin (TRPY) in multiple infection models**

A: Schematic of *K. pneumoniae* lung infection model. Mice (*n*=7) were intranasally infected with 1×10^7 CFU/mL of *K. pneumoniae* (clinical strain R62), treated 2 h post-infection, and analyzed 18 h post-treatment. B: Pulmonary bacterial burden in *K. pneumoniae*-infected untreated mice (vehicle) and mice treated with TRPY (2 mg/kg), or colistin (2 mg/kg). C: Pro-inflammatory cytokine levels (MCP-1, IL-6, TNF-α, IL-1β) in lung homogenates from infected mice following treatment. D: Representative H&E-stained lung sections (scale bar: 50 μmol/L) from healthy, infected, TRPY-treated (2 mg/kg), and colistin-treated (2 mg/kg) mice. E–G: Bacterial burden in peritoneal lavage fluid, liver, and kidneys, respectively, from mice (*n*=6) with MRSA peritoneal infection (1×10^8 CFU/mL) with vehicle (infected-untreated) or TRPY treatment (10 mg/kg). H: Representative H&E-stained kidney and liver sections from healthy, infected, vehicle-treated, or TRPY-treated (10 mg/kg) mice. I: Schematic of LPS-induced septic shock. J: Pro-inflammatory cytokine levels (IL-6, MCP-1, TNF-α, IL-1β) in serum from mice (*n*=5) challenged with LPS alone or LPS plus TRPY, LL-37, or colistin (all 10 mg/kg). Data are presented as mean±SEM. *: $P<0.05$; **: $P<0.01$; ***: $P<0.001$; ****: $P<0.0001$ vs. control or LPS-only control; ns: Not significant.

attribute for preventing the development of resistance. Time-kill kinetics demonstrated complete bacterial elimination within 60 min at 2 μmol/L, in contrast to the conventional antibiotic gentamicin, which required 10-fold higher concentrations and longer exposure time. This rapid, concentration-dependent bactericidal effect, combined with membrane disruption, ROS generation, and potential DNA interaction, indicates a multitarget mechanism that significantly reduces the likelihood of resistance emergence, a critical consideration given the current antimicrobial resistance crisis.

Most clinically significant is the potent activity of TRPY against biofilms and persister cells, achieving 95% inhibition of biofilm formation and complete eradication of persister cells at 8× MIC. These findings are promising given that conventional antibiotics exhibit limited efficacy against persister cells, which often underlie treatment failure and infection recurrence due to metabolic dormancy. The comprehensive antibiofilm and antipersister properties of TRPY suggest a broad-spectrum

mechanism of action that targets fundamental bacterial structures or processes conserved across diverse species. Additionally, the dual antimicrobial and immunomodulatory properties, as evidenced by the significant reduction in pro-inflammatory cytokines (IL-1β, TNF-α, and IL-6) and LPS neutralization, provide therapeutic advantages particularly relevant for managing severe infections complicated by excessive inflammation, such as sepsis.

Safety profiling revealed low hemolytic activity (<10%), high mammalian cell viability (>80%), and no detectable toxicity *in vivo*, indicating strong selectivity for bacterial over mammalian membranes. TRPY also significantly reduced bacterial burden in murine models of *K. pneumoniae* pulmonary and MRSA peritoneal infections, while outperforming LL-37 and colistin in suppressing inflammation in endotoxemia. The integration of broad-spectrum antimicrobial activity, rapid bactericidal kinetics, biofilm and persister cell clearance, host immunomodulation, and favorable safety profile of TRPY represents a significant advancement in addressing the global challenge of antimicrobial resistance via innovative structure-based design approaches.

Despite these promising findings, several limitations must be acknowledged. Although TRPY showed moderate proteolytic resistance, degradation over extended periods suggests that optimization strategies, such as cyclization, D-amino acid incorporation, or lipidation, may be necessary to further enhance stability. Furthermore, comprehensive immunological assessments, including antibody formation and hypersensitivity reactions, remain to be evaluated. Additionally, the rapid clearance observed may require multiple dosing or sustained-release formulations to maintain therapeutic levels in systemic infections. Moving forward, translational efforts should focus on evaluating the potential for resistance development over long-term exposure and optimizing pharmacokinetics through nanoparticle encapsulation or depot formulations. This will also involve assessing long-term safety and immunogenicity in larger animal models, as well as investigating combination regimens with conventional antibiotics to enhance efficacy and minimize resistance development.

SUPPLEMENTARY DATA

Supplementary data to this article can be found online.

COMPETING INTERESTS

The authors declare that they have no competing interests.

AUTHORS' CONTRIBUTIONS

R.L. conceptualized and supervised the project. J.M. designed and performed most of the experiments. D.A.T., Y.W., D.A., M.Y., B.B.M., and M.K. contributed to the animal experiments and data analysis. J.M., Z.Y.W., and Q.M.L. wrote and prepared the manuscript. All authors read and approved the final version of the manuscript.

REFERENCES

Armstrong CT, Mason PE, Anderson JLR, et al. 2016. Arginine side chain interactions and the role of arginine as a gating charge carrier in voltage sensitive ion channels. *Scientific Reports*, **6**(1): 21759.

Balasco N, Altamura D, Scognamiglio PL, et al. 2024. Self-assembled materials based on fully aromatic peptides: the impact of tryptophan, tyrosine, and dopa residues. *Langmuir*, **40**(2): 1470–1486.

Brandenburg K, Heinbockel L, Correa W, et al. 2016. Peptides with dual mode of action: killing bacteria and preventing endotoxin-induced sepsis. *Biochimica et Biophysica Acta (BBA) - Biomembranes*, **1858**(5): 971–979.

Bulet P, Stöcklin R, Menin L. 2004. Anti-microbial peptides: from invertebrates to vertebrates. *Immunological Reviews*, **198**(1): 169–184.

Cavaillon JM. 2018. Exotoxins and endotoxins: inducers of inflammatory cytokines. *Toxicon*, **149**: 45–53.

Chairatana P, Nolan EM. 2017. Human α-defensin 6: a small peptide that self-assembles and protects the host by entangling microbes. *Accounts of Chemical Research*, **50**(4): 960–967.

Chen SN, Tan Y, Xiao XC, et al. 2021. Deletion of TLR4 attenuates lipopolysaccharide-induced acute liver injury by inhibiting inflammation and apoptosis. *Acta Pharmacologica Sinica*, **42**(10): 1610–1619.

Chou SL, Guo HT, Zingl FG, et al. 2023. Synthetic peptides that form nanostructured micelles have potent antibiotic and antibiofilm activity against polymicrobial infections. *Proceedings of the National Academy of Sciences of the United States of America*, **120**(4): e2219679120.

Chu H, Pazgier M, Jung G, et al. 2012. Human α-defensin 6 promotes mucosal innate immunity through self-assembled peptide nanonets. *Science*, **337**(6093): 477–481.

Chu HL, Yu HY, Yip BS, et al. 2013. Boosting salt resistance of short antimicrobial peptides. *Antimicrobial Agents and Chemotherapy*, **57**(8): 4050–4052.

Chung PY. 2016. The emerging problems of *Klebsiella pneumoniae* infections: carbapenem resistance and biofilm formation. *FEMS Microbiology Letters*, **363**(20): fnw219.

Ciesielska A, Matyjek M, Kwiatkowska K. 2021. TLR4 and CD14 trafficking and its influence on LPS-induced pro-inflammatory signaling. *Cellular and Molecular Life Sciences*, **78**(4): 1233–1261.

Craft KM, Nguyen JM, Berg LJ, et al. 2019. Methicillin-resistant *Staphylococcus aureus* (MRSA): antibiotic-resistance and the biofilm phenotype. *MedChemComm*, **10**(8): 1231–1241.

Deslouches B, Di YP. 2017. Antimicrobial peptides with selective antitumor mechanisms: prospect for anticancer applications. *Oncotarget*, **8**(28): 46635–46651.

Deslouches B, Phadke SM, Lazarevic V, et al. 2005. De novo generation of cationic antimicrobial peptides: influence of length and tryptophan substitution on antimicrobial activity. *Antimicrobial Agents and Chemotherapy*, **49**(1): 316–322.

Duan BH, Zeng XJ, Peng JP. 2025. Advances in genotypic antimicrobialresistance testing: a comprehensive review. *Science China Life Sciences*, **68**(1): 130–143.

Eisenberg DS, Sawaya MR. 2017. Structural studies of amyloid proteins at the molecular level. *Annual Review of Biochemistry*, **86**(1): 69–95.

Ernst CM, Braxton JR, Rodriguez-Osorio CA, et al. 2020. Adaptive evolution of virulence and persistence in carbapenem-resistant *Klebsiella pneumoniae*. *Nature Medicine*, **26**(5): 705–711.

Glossop HD, De Zoysa GH, Hemar Y, et al. 2019. Battacin-inspired ultrashort peptides: nanostructure analysis and antimicrobial activity. *Biomacromolecules*, **20**(7): 2515–2529.

Greenwald J, Riek R. 2010. Biology of amyloid: structure, function, and regulation. *Structure*, **18**(10): 1244–1260.

Hamley IW. 2022. Peptides for vaccine development. *ACS Applied Bio Materials*, **5**(3): 905–944.

Harms A, Maisonneuve E, Gerdes K. 2016. Mechanisms of bacterial persistence during stress and antibiotic exposure. *Science*, **354**(6318): aaf4268.

Hossain TJ. 2024. Methods for screening and evaluation of antimicrobial activity: a review of protocols, advantages, and limitations. *European Journal of Microbiology and Immunology*, **14**(2): 97–115.

Huang XC, Li GL. 2023. Antimicrobial peptides and cell-penetrating peptides: non-antibiotic membrane-targeting strategies against bacterial infections. *Infection and Drug Resistance*, **16**: 1203–1219.

Jafari F, Elyasi S. 2021. Prevention of colistin induced nephrotoxicity: a

review of preclinical and clinical data. *Expert Review of Clinical Pharmacology*, **14**(9): 1113–1131.
Jan AT. 2017. Outer membrane vesicles (OMVs) of gram-negative bacteria: a perspective update. *Frontiers in Microbiology*, **8**: 1053.
Khemaissa S, Walrant A, Sagan S. 2022. Tryptophan, more than just an interfacial amino acid in the membrane activity of cationic cell-penetrating and antimicrobial peptides. *Quarterly Reviews of Biophysics*, **55**: e10.
Kim SJ, Kang TB, Kim DH, et al. 2022. 10-mer and 9-mer WALK peptides with both antibacterial and anti-inflammatory activities. *Antibiotics*, **11**(11): 1588.
Ko KS. 2017. The contribution of capsule polysaccharide genes to virulence of *Klebsiella pneumoniae*. *Virulence*, **8**(5): 485–486.
Lai ZH, Jian Q, Li GY, et al. 2021. Self-assembling peptide dendron nanoparticles with high stability and a multimodal antimicrobial mechanism of action. *ACS Nano*, **15**(10): 15824–15840.
Lei J, Sun LC, Huang SY, et al. 2019. The antimicrobial peptides and their potential clinical applications. *American Journal of Translational Research*, **11**(7): 3919–3931.
Li YS, Jia QY, Liu NX, et al. 2025. Peptide RL-QN15 regulates functions of epidermal stem cells to accelerate skin wound regeneration via the FZD8/β-Catenin axis. *Exploration*, 20240090.
Liu CB, Shan B, Bai HM, et al. 2015. Hydrophilic/hydrophobic characters of antimicrobial peptides derived from animals and their effects on multidrug resistant clinical isolates. *Zoological Research*, **36**(1): 41–47.
Ma XX, Yang N, Mao RY, et al. 2024. Self-assembly antimicrobial peptide for treatment of multidrug-resistant bacterial infection. *Journal of Nanobiotechnology*, **22**(1): 668.
Mazgaeen L, Gurung P. 2020. Recent advances in lipopolysaccharide recognition systems. *International Journal of Molecular Sciences*, **21**(2): 379.
Meinberger D, Drexelius MG, Grabeck J, et al. 2023. Modified CLEC3A-derived antimicrobial peptides lead to enhanced antimicrobial activity against drug-resistant bacteria. *Antibiotics*, **12**(10): 1532.
Miller WR, Arias CA. 2024. ESKAPE pathogens: antimicrobial resistance, epidemiology, clinical impact and therapeutics. *Nature Reviews Microbiology*, **22**(10): 598–616.
Mollica A, Macedonio G, Stefanucci A, et al. 2018. Arginine-and lysine-rich peptides: synthesis, characterization and antimicrobial activity. *Letters in Drug Design & Discovery*, **15**(3): 220–226.
Mwangi J, Kamau PM, Thuku RC, et al. 2023. Design methods for antimicrobial peptides with improved performance. *Zoological Research*, **44**(6): 1095–1114.
Mwangi J, Yin YZ, Wang G, et al. 2019. The antimicrobial peptide ZY4 combats multidrug-resistant *Pseudomonas aeruginosa* and *Acinetobacter baumannii* infection. *Proceedings of the National Academy of Sciences of the United States of America*, **116**(52): 26516–26522.
Niu HX, Gu JY, Zhang Y. 2024. Bacterial persisters: molecular mechanisms and therapeutic development. *Signal Transduction and Targeted Therapy*, **9**(1): 174.
Okesola BO, Mata A. 2018. Multicomponent self-assembly as a tool to harness new properties from peptides and proteins in material design. *Chemical Society Reviews*, **47**(10): 3721–3736.
Rambaran RN, Serpell LC. 2008. Amyloid fibrils: abnormal protein assembly. *Prion*, **2**(3): 112–117.
Russo TA, Marr CM. 2019. Hypervirulent *Klebsiella pneumoniae*. *Clinical Microbiology Reviews*, **32**(3): e00001–19.
Sancho-Vaello E, François P, Bonetti EJ, et al. 2017. Structural remodeling and oligomerization of human cathelicidin on membranes suggest fibril-like structures as active species. *Scientific Reports*, **7**(1): 15371.
Sancho-Vaello E, Gil-Carton D, François P, et al. 2020. The structure of the antimicrobial human cathelicidin LL-37 shows oligomerization and channel formation in the presence of membrane mimics. *Scientific Reports*, **10**(1): 17356.
Selvarajan V, Tram NDT, Xu J, et al. 2023. Stapled β-hairpin antimicrobial peptides with improved stability and activity against drug-resistant Gram-negative bacteria. *Journal of Medicinal Chemistry*, **66**(13): 8498–8509.
Shahmiri M, Enciso M, Adda CG, et al. 2016. Membrane core-specific antimicrobial action of cathelicidin LL-37 peptide switches between pore and nanofibre formation. *Scientific Reports*, **6**(1): 38184.
Sieprawska-Lupa M, Mydel P, Krawczyk K, et al. 2004. Degradation of human antimicrobial peptide LL-37 by *Staphylococcus aureus*-derived proteinases. *Antimicrobial Agents and Chemotherapy*, **48**(12): 4673–4679.
Singh S, Datta S, Narayanan KB, et al. 2021. Bacterial exo-polysaccharides in biofilms: role in antimicrobial resistance and treatments. *Journal of Genetic Engineering and Biotechnology*, **19**(1): 140.
Sinha NJ, Langenstein MG, Pochan DJ, et al. 2021. Peptide design and self-assembly into targeted nanostructure and functional materials. *Chemical Reviews*, **121**(22): 13915–13935.
Skwarczynski M, Toth I. 2016. Peptide-based synthetic vaccines. *Chemical Science*, **7**(2): 842–854.
Wang CK, King GJ, Conibear AC, et al. 2016. Mirror images of antimicrobial peptides provide reflections on their functions and amyloidogenic properties. *Journal of the American Chemical Society*, **138**(17): 5706–5713.
Wang JJ, Song J, Yang ZY, et al. 2019. Antimicrobial peptides with high proteolytic resistance for combating gram-negative bacteria. *Journal of Medicinal Chemistry*, **62**(5): 2286–2304.
Wu ZX, Cai Y, Han YJ, et al. 2024. Development of α-Helical antimicrobial peptides with imperfect amphipathicity for superior activity and selectivity. *Journal of Medicinal Chemistry*, **67**(21): 19561–19572.
Yao LFK, Liu QY, Lei ZX, et al. 2023. Development and challenges of antimicrobial peptide delivery strategies in bacterial therapy: a review. *International Journal of Biological Macromolecules*, **253**: 126819.
Yu WK, Wang JJ, Wang ZH, et al. 2021. PEGylation of the antimicrobial peptide PG-1: a link between propensity for nanostructuring and capacity of the antitrypsin hydrolytic ability. *Journal of Medicinal Chemistry*, **64**(14): 10469–10481.
Zare-Zardini H, Saberian E, Jenča A, et al. 2024. From defense to offense: antimicrobial peptides as promising therapeutics for cancer. *Frontiers in Oncology*, **14**: 1463088.
Zeth K, Sancho-Vaello E. 2021. Structural plasticity of LL-37 indicates elaborate functional adaptation mechanisms to bacterial target structures. *International Journal of Molecular Sciences*, **22**(10): 5200.
Zhang JK, Liu SN, Li H, et al. 2020. Tryptophan-based self-assembling peptides with bacterial flocculation and antimicrobial properties. *Langmuir*, **36**(38): 11316–11323.